AIP | Applied Physics Letters

Modeling of filamentary resistive memory by concentric cylinders with variable conductivity

Andrew J. Lohn, Patrick R. Mickel, and Matthew J. Marinella

Citation: Applied Physics Letters **105**, 183511 (2014); doi: 10.1063/1.4901351
View online: http://dx.doi.org/10.1063/1.4901351
View Table of Contents: http://scitation.aip.org/content/aip/journal/apl/105/18?ver=pdfcov
Published by the AIP Publishing

Modeling of filamentary resistive memory by concentric cylinders with variable conductivity

Andrew J. Lohn,[a] Patrick R. Mickel, and Matthew J. Marinella
Sandia National Laboratories, Albuquerque, New Mexico 87185, USA

(Received 14 August 2014; accepted 27 October 2014; published online 7 November 2014)

We demonstrate a method for modeling memristors (resistive random access memories) where the filament is composed of a set of nanoscale or sub-nanoscale concentric cylinders, each having its own conductivity. This approach allows for the inclusion of multiple state variables, which, we show experimentally, can be used to control electrical behavior. The simulations accurately reproduce the current-voltage hysteresis loop as well as these more complex experimental behaviors resulting from intricate switching histories. The simulations can be both static and dynamic, and are based upon physical design parameters, so optimized values from simulation can be easily linked to device design. © *2014 AIP Publishing LLC*. [http://dx.doi.org/10.1063/1.4901351]

Memristors or resistive random access memories (RRAM) change their resistance in a non-volatile manner in response to applied electrical signal.[1,2] They are promising as non-volatile memories due to excellent speed,[3] size,[4] power consumption,[5] and endurance,[6] but their electrical behavior is novel in passive circuit elements and is therefore unfamiliar to most circuit designers. Despite their relative youth, these devices have already prompted significant interest and promise in applications such as threshold logic[7,8] and neuromorphic computing.[9–11] In order to make progress in developing these circuits and to create new circuits that utilize the novel properties of these devices, good computational simulators are needed. Although many memristive or RRAM simulators exist,[12–15] many of these simulators are based on the idealized memristor equations[16] and therefore do not capture important features of real devices such as thresholding[17] and bounded resistance ranges.[18] The authors also are not aware of any model outside of full finite-element simulation[19] capable of incorporating multiple state variables which have been shown experimentally[20] to significantly alter device behavior. Additionally, convergence can be a problem for some of the simulators, making the simulation of large scale circuits (such as crossbar arrays) impossible. Finally, an ideal simulator would be based on physical parameters so that optimal properties identified in simulation can be communicated directly to the fabrication team to accelerate real device, circuit, and system development. Here, we present a computationally compact simulator based on physical design parameters that is capable of reproducing the complex switching characteristics that arise from complex switching histories.

A recent analytical model was developed that provides the steady state solution for memristive switching as a function of applied power.[21] The model also identified additional state variables that can be used to control electrical characteristics such as the switching threshold.[20] This steady state approach has been validated for even the fastest data recorded to date,[21] so a time-varying output can be accurately calculated from a time-varying input signal by finding the steady state solution at every step in time. This approach greatly simplifies the simulation by eliminating both the need to specify a time-dependence for the memristor response and the associated integration required to calculate the memristance.

The model consists of a set of concentric rings (referred to as shells) as shown in Fig. 1. Each shell has its own resistance, and the total device resistance is calculated as the parallel sum of the individual shell resistances. Each shell has a variable quantity that is meant to represent the concentration of oxygen vacancies. The conductivity of each shell is calculated according to Eq. (1) from the concentration variable and the applied voltage as a weighted sum of an Ohmic term and a Poole-Frenkel term, which provides a nonlinear conduction mechanism[22]

$$\sigma = \sigma_{sat}\left[\frac{C - C_{min}}{C_{min}} + \left(1 - \frac{C - C_{min}}{C_{min}}\right) aVe^{b\sqrt{V}}\right]. \quad (1)$$

In Eq. (1), σ_{sat} is the saturation conductivity, C_{min} is the minimum concentration (50 units), and a and b are Poole-Frenkel coefficients. The Poole-Frenkel term

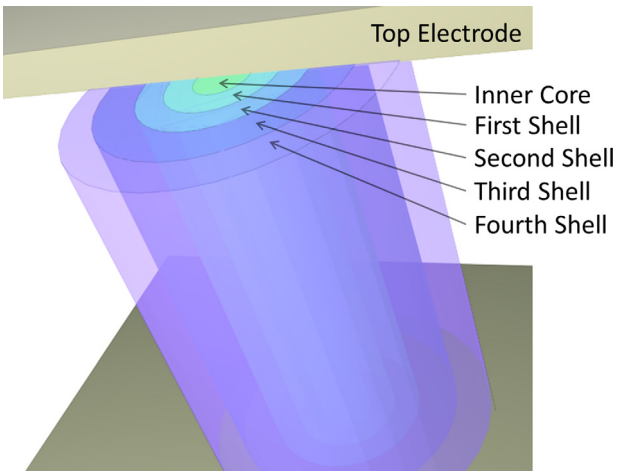

FIG. 1. Half of the top electrode is removed to show a conducting filament modeled using concentric shells. Each shell has its own concentration and therefore conductivity. The resistance of the device is calculated as the parallel sum of the shell resistances.

[a]ajlohn@sandia.gov

neglects substantial self-heating effects and may not represent the correct physics, however, it is sufficiently representative for most applications; where other nonlinearity mechanisms are preferred that they can be easily exchanged in Eq. (1).[23]

In real devices, the concentration of oxygen vacancies cannot exceed some saturation value which results in a corresponding saturation conductivity[24] that can be measured electrically via a hysteresis loop.[21] In our simulations, we normalized the conductivity of the Ohmic term to the saturation conductivity. The Poole-Frenkel term was fit to the completely switched OFF state with the concentration variable set to the minimum concentration value, thereby identifying the coefficients a and b in $I = aVe^{b\sqrt{V}}$. The conductivity of each shell is then calculated from Eq. (1), where the concentration variable C is allowed to vary.

Allowing the conductivity of each shell to change by modulating its concentration value leads to resistance changes in the device. Deciding which shells are allowed to change, and by how much, is the primary objective of the simulation. The analytical model described earlier provides the limiting expressions for both ON and OFF switching by specifying the minimum amount of power required to allow switching. At powers less than those specified by Eq. (2), the temperature inside the device is too low to allow for ionic motion and no switching occurs. Equation (2) can be written in a simplified form for ON and OFF switching in Eqs. (3a) and (3b), respectively

$$P = \frac{(T_{crit} - T_{RT})/R}{\frac{\sigma d_e}{2k_e d_o} - \frac{r_f^2}{8L_{WF}T_c d_o^2}}, \tag{2}$$

$$P_{ON} = \frac{A_r(T_{crit} - T_{RT})}{R - R_{min}}, \tag{3a}$$

$$P_{OFF} = \frac{A_\sigma(T_{crit} - T_{RT})}{R_{max} - R}. \tag{3b}$$

In the above equations, P is the applied electrical power and R is the resistance. T_{crit} is the critical temperature for ion motion and T_{RT} is the ambient temperature of the device. d_e is electrode thickness, k_e is electrode thermal conductivity, d_o is thickness of the oxide insulator, r_f is filament radius, r_f is the filament radius, σ_{max} is the conductivity corresponding to the saturation concentration, and L_{WF} is the Wiedemann-Franz constant.

During ON switching, vacancies enter the filament in the center (where temperature and therefore ionic mobility is highest) until the central region saturates. Continued injection of vacancies forces the saturated region to expand, since it is not possible for them to be incorporated in the already saturated region. In the simulation, ON switching progresses by increasing the number of saturated shells, starting from the center, until Eq. (3a) is satisfied. If the power supplied is less than the right hand side of Eq. (3a), then insufficient power is being supplied to achieve thermal activation and to allow ions to move. During OFF switching, if sufficient power is supplied, the region of highest concentration becomes thermally activated and the concentration of vacancies within that entire region decreases until the power is no longer sufficient for continued switching. The condition for OFF switching power is given in Eq. (3b). To summarize, for ON switching, the number of saturated shells is incremented until Eq. (3a) is satisfied and for OFF switching, the concentration of the group of shells with the highest concentration is decremented until the Eq. (3b) is satisfied.

For comparison to experiment, we used CMOS-compatible TaOx-based RRAM devices.[24,25] Values for σ_{max}, k_E, and T_{crit} were identified from fitting to the ON-switching data as in Ref. 21 and as shown in the inset of Fig. 2(b). The Poole-Frenkel a and b parameters were fit from the OFF state. All other parameters are known from the fabrication process. All parameters are included in the simulation code provided in the supporting information along with the code used to extract them from the current-voltage data.[26] As seen in Fig. 2, the simulation is able to reproduce the current-voltage hysteresis loop with reasonable accuracy in terms of the resistance values for ON and OFF states, the threshold values for ON and OFF switching, and the range of resistance states throughout switching. The data also also shown in power-resistance coordinates which are the more natural frame for Eqs. (2) and (3).

Three regions in Fig. 2 stand out as being inexact. The first is the nonlinear conductivity of the OFF state. As described earlier, the Poole-Frenkel mechanism may not be the most appropriate physical mechanism and we have ignored substantial self-heating, but this approach is simple and sufficiently accurate for most applications. Second, the negative sloping region at the start of ON switching is not captured exactly. That region corresponds to increases in concentration prior to reaching the saturation concentration of the core region[27] which is not included in this simulation. That behavior can be included by allowing a group of core

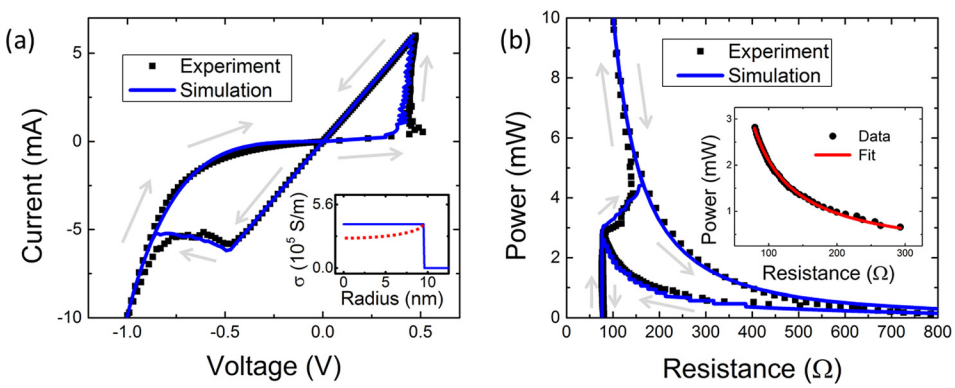

FIG. 2. A current-voltage hysteresis loop can be reproduced very accurately using the shell-based simulator once the device parameters are found (inset of part (b)). The current-voltage traces (a) can also be represented in power-resistance coordinates (b) that are more natural to the equations used in the simulation. The inset of part a shows a conductivity profile during OFF switching in simulation (blue solid) and the core depression that is expected in real devices (red dotted).

shells to increase concentration gradually instead of proceeding immediately to saturation, but the additional steps add computational time, and it is difficult to estimate the number of shells that constitute the core. Third, the discrepancy during OFF-switching is due to an approximation made during simulation; the simulation decrements conductivity uniformly, but in a real device the conductivity will decrease from the center shells first[20] and their concentration will stay slightly lower than the rest of the filament. This concept is illustrated in the inset of Fig. 2(a), where the radial conductivity profile is depicted for a simulated device (solid blue) and device with decreased core concentration (dotted red) as might be expected in reality. We refer to this difference as the uniformly decreasing concentration assumption (UDCA), and, although it leads to inexact OFF-switching behavior, it is sufficiently accurate for most cases.

Interestingly, in both the simulation and the experiment, there is noise during switching. During OFF switching, the noise is controlled by the step size in the concentration variable, whereas during ON switching, it is controlled by the size of the shell radius. In Fig. 2, there are 50 concentration steps, which may be larger than in a real device, leading to small noise in the simulation. The shell radius was set to 1 angstrom (approximately atomic scale), and the noise is comparable to experiment, suggesting that the ON switching noise may be related to the atomic nature of radius expansion.

Demonstrating simple behavior, where the device is cycled between consistent endpoints (as in Fig. 2), is a mandatory requirement of simulation but a main benefit of this shell-based approach is the ability to rapidly simulate more complex histories and behaviors. An example of this complex behavior is shown in Fig. 3, where partial OFF and ON switching is used to create new features in the current-voltage relationship. The conductivity profile of the filament following each half-cycle is also provided as insets throughout the progression to show how the device configuration evolves. In this example, a device with a particularly poor UDCA was chosen to illustrate the limitations of our approach. In parts (a) and (b), a simple hysteresis loop is shown where thresholding and resistance values are accurately replicated, but the exaggerated upward curl during OFF switching is not reproduced accurately because of the poor UDCA. In parts (c) and (d), a complicated history is developed by only partially OFF switching the device. Due to the difference in OFF switching behavior caused by the poor UDCA, the simulator required slightly higher voltage to replicate the experiment but stills shows very similar

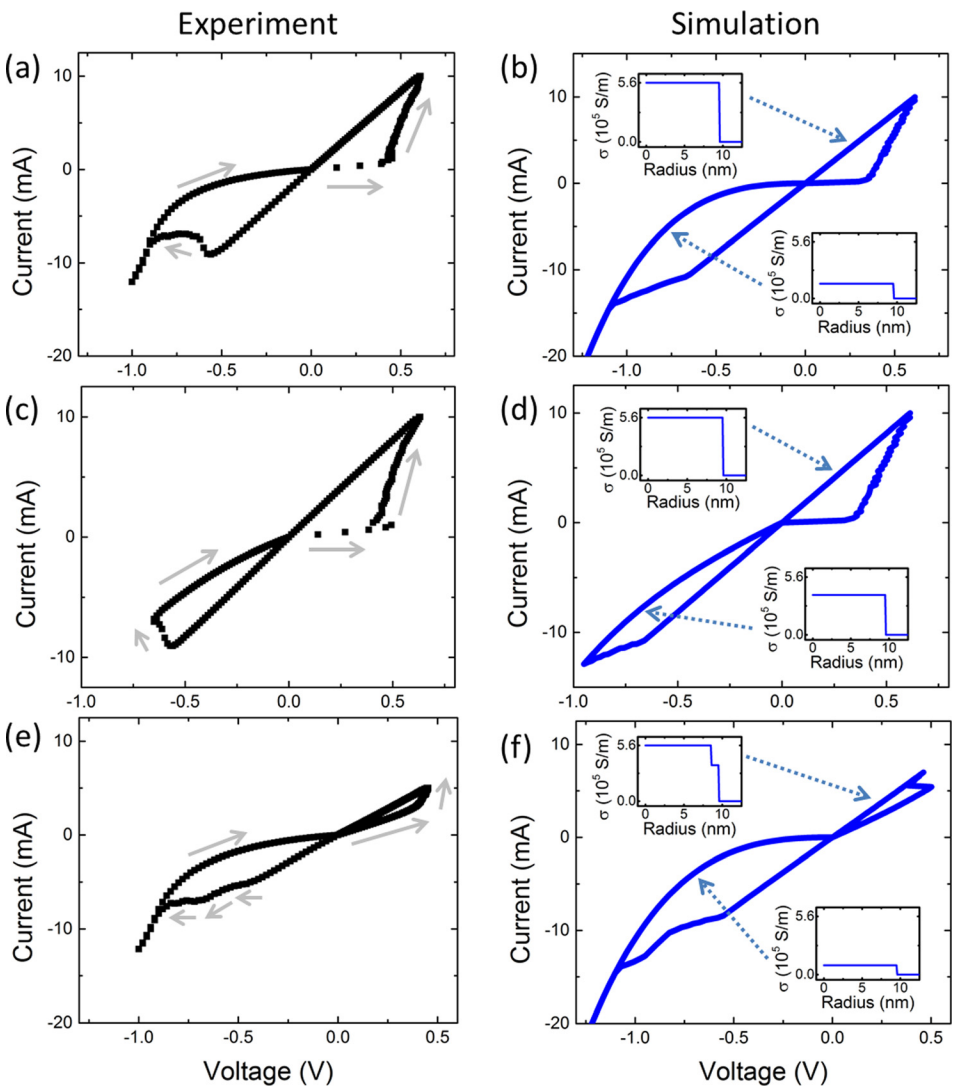

FIG. 3. Device behavior can depend on complex histories. Parts (a) and (b) show a simple hysteresis loop. Partial OFF switching ((c) and (d)) followed by partial ON switching ((e) and (f)) leads to a step in the conductivity profile (upper inset of (f)) which causes a bump in the OFF switching ((e) and (f)). Experimental data are shown in the left column and simulation on the right with the conductivity profile shown as insets after every half cycle.

behavior in at least a qualitative sense. Partial OFF switching also leads to decreased nonlinearity seen in both experiment and simulation. As shown in part (e), this complex history leads to a change in threshold for ON switching and a clear bump in the OFF switching experiment. Both of these behaviors are captured well by the simulator in Fig. 3(f).

These complex switching characteristics arise because there is more than one state variable in both the real devices and the simulator. The radius of the filament is allowed to change but so is the conductivity of any region within that radius. The conductivity of each shell is a state variable, and so very intricate behavior can be created in real devices and represented with shell-based simulation. These types of effects can be used to store large amounts of information in multi-dimensional information spaces[20] or to control thresholds or learning rates in neural systems.[11] The specific conductivity profiles for this series of configurations are shown as insets in Fig. 3, but much more complicated profiles can be created to provide more interesting electrical behavior. In the case of the bump in OFF switching in Figs. 3(e) and 3(f), the two-level conductivity profile in the top inset of Fig. 3(f) is the important characteristic. During OFF switching, the inner section starts switching first until its concentration decreases to the level of the outer section. At that point, more power is required before switching can continue so the device is temporarily stabilized, leading to the bump in the I-V loop.

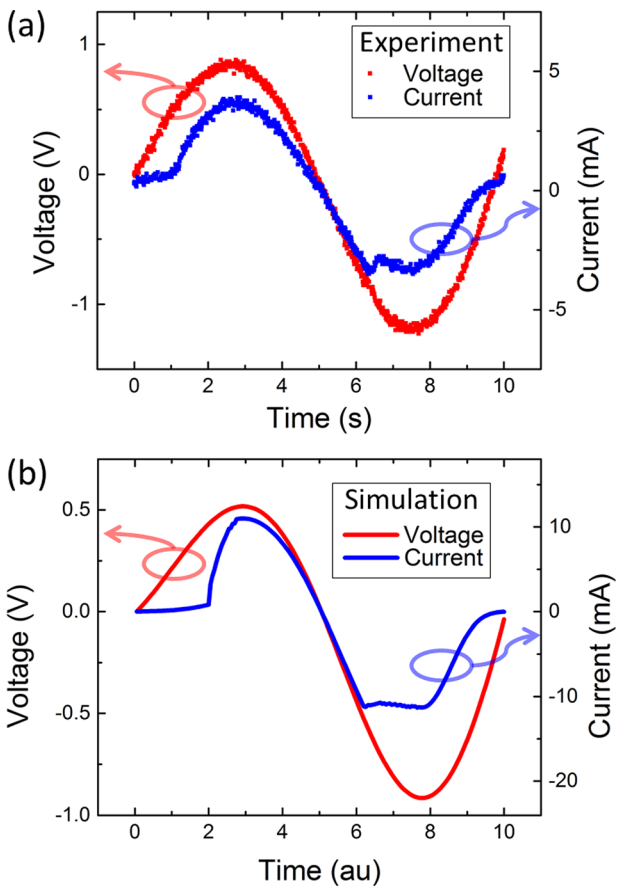

FIG. 4. The steady-state simulator can be used to provide the output waveform for a time-varying input signal. A sine wave with increasing amplitude is used as an input signal for an experimental demonstration (a) and a simulation (b).

Often the goal of a device simulation is not to generate the current-voltage relation but to study the output waveform for a given input waveform.[28,29] An example is shown in Fig. 4 where a sinusoid with increasing amplitude is used as the input signal for an experimental curve in Fig. 4(a) and a simulation in Fig. 4(b). The experimental current was measured using a 100 Ω series resistor. This experiment was done at very slow timescales (~10 s period) to illustrate the steady-state nature of both the simulation and the experiment. As mentioned in the introduction, the equations used in this model have been validated for the fastest data recorded to date (~1 ns) (Ref. 21) so higher-speed simulations are also possible, though they may require increasing the value of the activation temperature slightly.

In summary, a modeling approach has been developed for simulating memristor or RRAM electrical behavior based on modulation of the oxygen concentration within a conducting filament composed of many concentric shells. This approach is able to accurately reproduce simple electrical behavior such as the current-voltage hysteresis loop and basic time-varying responses, but it is also able to reproduce much more complicated behavior. By allowing the conductivity of each shell to vary separately, complex device histories and conductivity profiles can be generated which lead to intricate characteristics that are observed in corresponding experiments. Also, since any change or optimization in the simulation is done by changing physical design parameters such as thickness or thermal conductivity, optimized parameters from simulation can be communicated directly to designers to help create a wide range of device properties, electrical characteristics, and even systems level designs.

The authors would like to thank Jim Stevens and the Sandia MESA Fab for their work in fabricating devices used in this study. This work was funded by Sandia's Laboratory Directed Research and Development (LDRD) program. Sandia National Laboratories is a multi-program laboratory managed and operated by Sandia Corporation, a wholly owned subsidiary of Lockheed Martin Corporation, for the U.S. Department of Energy's National Nuclear Security Administration under contract DE-AC04-94AL85000.

[1]J. J. Yang, D. B. Strukov, and D. R. Stewart, "Memristive devices for computing," Nat. Nanotechnol. **8**, 13–24 (2013).
[2]P. R. Mickel, A. J. Lohn, and M. J. Marinella, "Memristive switching: physical mechanisms and applications," Mod. Phys. Lett. B **28**, 1430003 (2014).
[3]A. C. Torrezan, J. P. Strachan, G. Medeiros-Ribeiro, and R. S. Williams, "Sub-nanosecond switching of a tantalum oxide memristor," Nanotechnology **22**, 485203 (2011).
[4]A. J. Lohn, P. R. Mickel, and M. J. Marinella, "Analytical estimations for thermal crosstalk, retention and scaling limits in filamentary resistive memory," J. Appl. Phys. **115**, 234507 (2014).
[5]J. P. Strachan, A. C. Torrezan, G. Medeiros-Ribeiro, and R. S. Williams, "Measuring the switching dynamics and energy efficiency of tantalum oxide memristors," Nanotechnology **22**, 505402 (2011).
[6]M.-J. Lee, C. B. Lee, D. Lee, S. R. Lee, M. Chang, J. H. Hur, Y.-B. Kim, C.-J. Kim, D. H. Seo, S. Seo, U.-I. Chung, I.-K. Yoo, and K. Kim, "A fast, high-endurance and scalable non-volatile memory device made from asymmetric Ta_2O_{5-x}/TaO_{2-x} bilayer structures," Nat. Mater. **10**, 625–630 (2011).
[7]J. Rajendran, H. Manem, R. Karri, and G. S. Rose, "An energy-efficient memristive threshold logic circuit," IEEE Trans. Comput. **61**, 474–487 (2012).

[8]L. Gao, F. Alibart, and D. B. Strukov, "Programmable CMOS/Memristor Threshold Logic," IEEE Trans. Nanotechnol. **12**, 115–119 (2013).
[9]V. Y. Pershin and M. Di Ventra, "Experimental demonstration of associative memory with memristive neural networks," Neural Networks **23**, 881–886 (2010).
[10]S.-H. Jo, T. Chang, I. Ebong, B. B. Bhadviya, P. Mazumder, and W. Lu, "Nanoscale memristor device as synapse in neuromorphic systems," Nano Lett. **10**, 1297–1301 (2010).
[11]A. J. Lohn, P. R. Mickel, J. B. Aimone, E. P. Debenedictis, and M. J. Marinella, "Memristors as synapses in artificial neural networks: Biomimicry beyond weight change," in *Cybersecurity Systems for Human Cognition Augmentation* (Springer, 2014).
[12]S. Kvatinsky, E. G. Friedman, A. Kolodny, and U. C. Weiser, "TEAM: Threshold adaptive memristor model," IEEE Trans. Circuits Syst. **60**, 211–221 (2013).
[13]H. Li, P. Huang, B. Gao, B. Chen, X. Liu, and J. Kang, "A SPICE model of resistive random access memory for large-scale memory array simulation," IEEE Electron Device Lett. **35**, 211–213 (2014).
[14]Z. Biolek, D. Biolek, and V. Biolkova, "SPICE model of memristor with nonlinear dopant drift," Radioengineering **18**, 210–214 (2009).
[15]H. Abdalla and M. D. Pickett, "SPICE modeling of memristors," in *2011 IEEE International Symposium on Circuits and Systems (ISCAS)* (IEEE, 2011), pp. 1832–1835.
[16]L. O. Chua, "Memristor—The missing circuit element," IEEE Trans. Circuit Theory **18**, 507–519 (1971).
[17]F. Nardi, S. Larentis, S. Balatti, D. C. Gilmer, and D. Ielmini, "Resistive switching by voltage-driven ion migration in bipolar RRAM—Part I: Experimental study," IEEE Trans. Electron Devices **59**, 2461–2467 (2012).
[18]A. J. Lohn, P. R. Mickel, and M. J. Marinella, "Dynamics of percolative breakdown mechanism in tantalum oxide resistive switching," Appl. Phys. Lett. **103**, 173503 (2013).
[19]S. Larentis, F. Nardi, S. Balatti, D. C. Gilmer, and D. Ielmini, "Resistive switching by voltage-driven ion migration in bipolar RRAM—Part II: Modeling," IEEE Trans. Electron Devices **59**, 2468–2475 (2012).
[20]A. J. Lohn, P. R. Mickel, C. D. James, and M. J. Marinella, "Degenerate Resistive Switching and Ultrahigh Density Storage in Resistive Memory," Appl. Phys. Lett. **105**, 103501 (2014).
[21]P. R. Mickel, A. J. Lohn, C. D. James, and M. J. Marinella, "Isothermal switching and detailed filament evolution in memristive systems," Adv. Mater. **26**, 4486–4490 (2014).
[22]P. R. Mickel, A. J. Lohn, B. J. Choi, J. J. Yang, M.-X. Zhang, M. J. Marinella, C. D. James, and R. S. Williams, "A physical model of switching dynamics in tantalum oxide memristive devices," Appl. Phys. Lett. **102**, 223502 (2013).
[23]S. M. Sze and K. K. Ng, *Physics of Semiconductor Devices*, 3rd ed. (John Wiley & Sons, 2007), p. 227.
[24]A. J. Lohn, J. E. Stevens, P. R. Mickel, D. R. Hughart, and M. J. Marinella, "A CMOS compatible, forming free TaOx ReRAM," ECS Trans. **58**, 59 (2013).
[25]A. J. Lohn and P. R. Mickel, "Optimizing TaOx memristor performance and consistency within the reactive sputtering "forbidden region"," Appl. Phys. Lett. **103**, 063502 (2013).
[26]See supplementary material at http://dx.doi.org/10.1063/1.4901351 for simulation and parameter extraction codes.
[27]A. J. Lohn, P. R. Mickel, and M. J. Marinella, "Mechanism of electrical shorting failure mode in resistive switching," J. Appl. Phys. **116**, 034506 (2014).
[28]L. Duan and L. Huang, "Periodicity and dissipativity for memristor-based mixed time-varying delayed neural networks via differential inclusions," Neural Networks **57**, 12–22 (2014).
[29]A. G. Radwan, M. A. Zidan, and K. N. Salama, "HP memristor mathematical model for periodic signals and DC," in *2010 53rd IEEE International Midwest Symposium on Circuits and Systems (MWSCAS)* (IEEE, 2010), pp. 861–864.